Abstracta

Ano XXVIII - N. 02

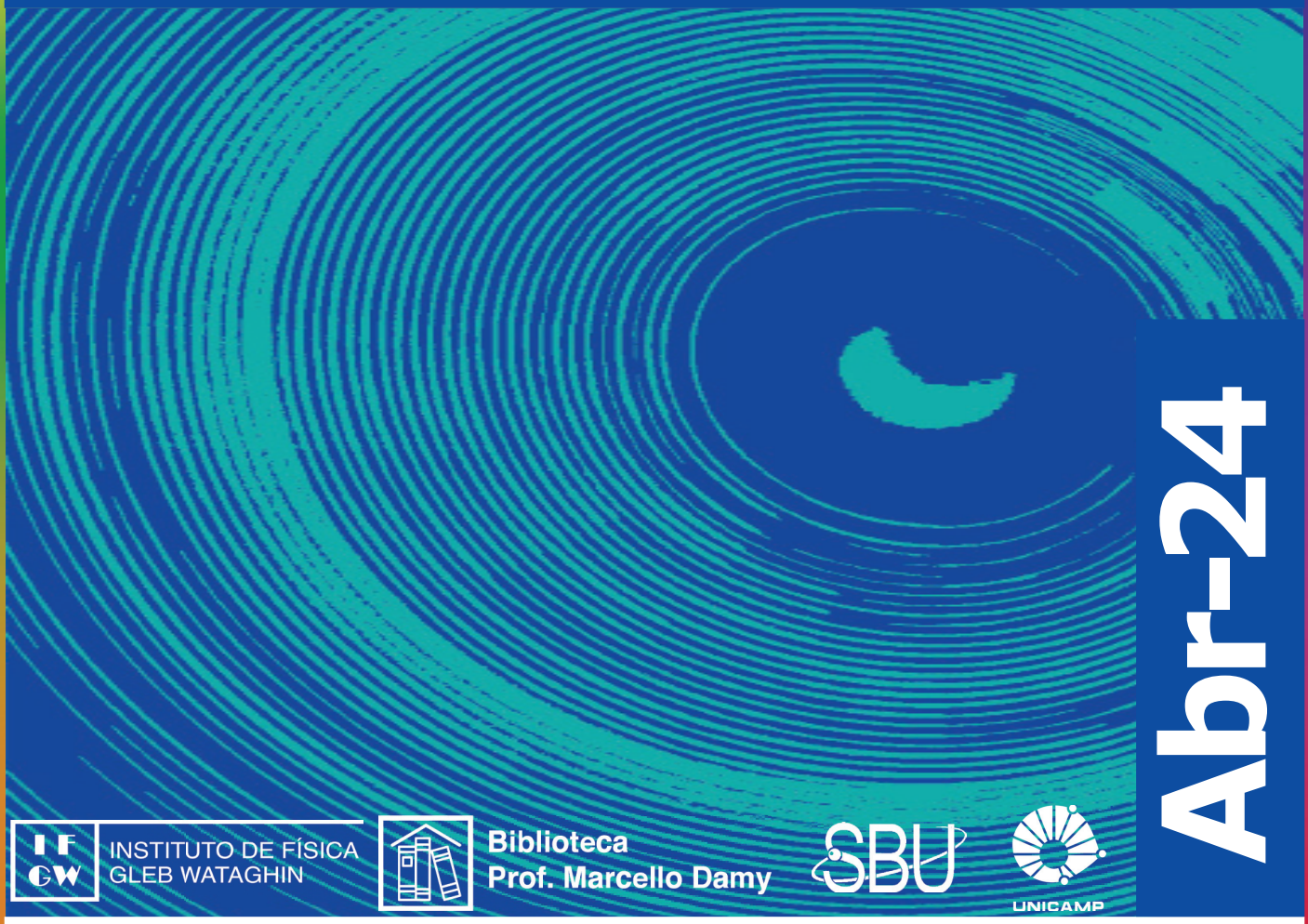

Artigos publicados - P017-2024 à P056-2024

Defesas de Dissertações do IFGW - D007-2024 à D10-2024

Defesas de Teses do IFGW - T004-2024 à T006-2024

Defesas do PECIM - P002-2024

Artigos publicados

[P017-2024] "All-fiber broadband spectral acousto-optic modulation of a tubular-lattice hollow-core optical fiber"

Silva, R. E. da; **Osório, J. H.*; Rodrigues, G. L.*;** Webb, D. J.; Gérôme, F.; Benabid, F.; **Cordeiro, C. M. B.*;** Franco, M. A. R.

We demonstrate a broadband acousto-optic notch filter based on a tubular -lattice hollow -core fiber for the first time to our knowledge. The guided optical modes are modulated by acoustically induced dynamic long -period gratings along the fiber. The device is fabricated employing a short interaction length (7.7 cm) and low drive voltages (10 V). Modulated spectral bands with 20 nm half -width and maximum depths greater than 60% are achieved. The resonant notch wavelength is tuned from 743 to 1355 nm (612 nm span) by changing the frequency of the electrical signal. The results indicate a broader tuning range compared to previous studies using standard and hollow -core fibers. It further reveals unique properties for reconfigurable spectral filters and fiber lasers, pointing to the fast switching and highly efficient modulation of all -fiber photonic devices.

OPTICS LETTERS 49[3], 690-693, 2024. DOI: 10.1364/OL.512222

[P018-2024] "Automatic detection of fake tweets about the COVID-19 Vaccine in Portuguese"

Geurgas, R.*; Tessler, L. R.*

The COVID-19 pandemic induced an unprecedented wave of disinformation in social media in Brazil. In particular, Twitter (currently X) was used to spread fake news about COVID-19 vaccines that helped to induce vaccine hesitation. This article presents a BERT-based neural network for the automatic detection of fake tweets. The optimized architecture relies upon BERTimbau, a BERT implementation pre-trained in Brazilian Portuguese, fine-tuned using three fully connected layers. All 2,857,908 tweets in Portuguese containing the word vacina (vaccine in Portuguese) were collected over 7 months. A random subset of 16,731 tweets was manually classified as real or fake. Of these, 2309 were discarded for not being about non-COVID-19 vaccines and 422 were discarded for containing irony. Of the remaining 14,000 tweets, 1144 were labeled fake and 12,856 were real. To balance the training dataset, the network was fine-tuned using the 1144 curated fake tweets and a random sample of 2000 real tweets. Optimal results were achieved by melting the last four layers of the BERTimbau. The best results obtained were 77.1% F1-score and 76.9% accuracy. These results are already acceptable for practical applications. They can be improved by increasing the size of the training dataset. A weighted 96.3% F1-score was obtained by training the same neural network architecture and hyperparameters with a larger curated balanced English language training dataset.

SOCIAL NETWORK ANALYSIS AND MINING 14[1], 55, 2024. DOI: 10.1007/s13278-024-01216-x

[P019-2024] "Characterizing two-mode-squeezed light from four-wave mixing in rubidium vapor for quantum sensing and information processing"

Araujo, L. E. E. de*; Zhou, Z. F.; DiMario, M.; Anderson, B. E.; Zhao, J.; Jones, K. M.; Lett, P. D.

We present a study of homodyne measurements of two-mode, vacuum-seeded, quadrature-squeezed light generated by four-wave mixing in warm rubidium vapor. Our results reveal that the vacuum squeezing can extend down to measurement frequencies of less than 1 Hz, and the squeezing bandwidth, similar to the seeded intensity-difference squeezing measured in this system, reaches up to approximately 20 MHz for typical pump parameters. By dividing the squeezing bandwidth into smaller frequency bins, we show that different sideband frequencies represent independent sources of two-mode squeezing. These properties are useful for quantum sensing and quantum information processing applications. We also investigate the impact of group velocity delays on the correlations in the system, which allows us to optimize the useful spectrum.

OPTICS EXPRESS 32[2], 1305-1313, 2024. DOI: 10.1364/OE.507727

[P020-2024] "Charged-particle production as a function of the relative transverse activity classifier in pp, p-Pb, and Pb-Pb collisions at the LHC'

Acharya, S.; Adamova, D.; **Chinellato, D. D.*; Guardiano, G. G.*; Liveraro, G. S. S.*; Takahashi, J.***; et al.
ALICE Collaboration

Measurements of charged-particle production in pp, p-Pb, and Pb-Pb collisions in the toward, away, and transverse regions with the ALICE detector are discussed. These regions are defined event-by-event relative to the azimuthal direction of the charged trigger particle, which is the reconstructed particle with the largest transverse momentum (p(trig) (T)) in the range 8 < p(trig) (T) < 15 GeV/c. The toward and away regions contain the primary and recoil jets, respectively; both regions are accompanied by the underlying event (UE). In contrast, the transverse region perpendicular to the direction of the trigger particle is dominated by the so-called UE dynamics, and includes also contributions from initial- and final-state radiation. The relative transverse activity classifier, R-T = N-ch(T)/< N--ch(T)>, is used to group events according to their UE activity, where < N-ch(T)> is the charged-particle multiplicity per event in the transverse region and.< N-ch(T)>. is the mean value over the whole analysed sample. The energy dependence of the R-T distributions in pp collisions at root s = 2.76, 5.02, 7, and 13TeV is reported, exploring the Koba-Nielsen-Olesen (KNO) scaling properties of the multiplicity distributions. The first measurements of charged-particle pT spectra as a function of RT in the three azimuthal regions in pp, p-Pb, and Pb--Pb collisions at root sNN = 5.02TeV are also reported. Data are compared with predictions obtained from the event generators PYTHIA 8 and EPOS LHC. This set of measurements is expected to contribute to the understanding of the origin of collective-like effects in small collision systems (pp and p-Pb).

JOURNAL OF HIGH ENERGY PHYSICS [1], 56, 2024. DOI: 10.1007/JHEP01(2024)056

[P021-2024] "Comparative Passivation of Si(100) by H2 and D2 Atmospheres under Simultaneous Xe+ Bombardment: An X-ray Photoelectron Spectroscopy Analysis"

Antunes, V. G.*; Jimenez, M. J. M.*; Cemin, F.*; Figueroa, C. A.; **Alvarez, F.***

This study presents a comparison of H-2 and D-2 passivation on Si(100) under simultaneous Xe+ ion bombardment. The impact of Xe+ ions causes significant damage to the substrate surface, leading to an increase in H-2 (D-2) retention as Si-H (Si-D) bonds. The ion bombardment conditions are precisely controlled using a Kaufman ion gun. The atomic concentrations on the surface of the sample were investigated by quasi-in situ X-ray photoelectron spectroscopy. A simple methodology is employed to estimate the H (D) chemical concentration and the cover ratio of the sample, with regard to the oxygen concentration through residual water chemisorption present in the vacuum vessel.

Differences in passivation are expected when using H-2 or D-2 atmospheres because their retained scission energies and physisorption properties differ. The results indicate an increase of the sticking coefficient for D-2 and H-2 under the ion bombardment. It is also found that the flux of H-2 (D-2) impinging on the surface contributes to play an important role in the whole process. Finally, a model is proposed to describe the phenomenon of the passivation of Si under Xe+ ion bombardment in the presence of H-2 (D-2).

LANGMUIR, 2024. DOI: 10.1021/acs.langmuir.3c03723. **Early Access Date:** FEB 2024

[P022-2024] "Constraining models for the origin of ultra-high-energy cosmic rays with a novel combined analysis of arrival directions, spectrum, and composition data measured at the Pierre Auger Observatory"

Halim, A. A.; Abreu, P.; **Bonneau Arbeletche, L.*; Chinellato, J. A.*; Oliveira Franco, D.*; Dobrigkeit, C.*; Fauth, A. C.*; Machado Payeras, A.*; Reginatto Akim, J. V.***; et al.
Pierre Auger Collaboration

The combined fit of the measured energy spectrum and shower maximum depth distributions of ultra-high-energy cosmic rays is known to constrain the parameters of astrophysical models with homogeneous source distributions. Studies of the distribution of the cosmic-ray arrival directions show a better agreement with models in which a fraction of the flux is non-isotropic and associated with the nearby radio galaxy Centaurus A or with catalogs such as that of starburst galaxies. Here, we present a novel combination of both analyses by a simultaneous fit of arrival directions, energy spectrum, and composition data measured at the Pierre Auger Observatory. The model takes into account a rigidity-dependent magnetic field blurring and an energy-dependent evolution of the catalog contribution shaped by interactions during propagation. We find that a model containing a flux contribution from the starburst galaxy catalog of around 20% at 40 EeV with a magnetic field blurring of around 20 degrees for a rigidity of 10EV provides a fair simultaneous description of all three observables. The starburst galaxy model is favored with a significance of 4.5 sigma (considering experimental systematic effects) compared to a reference model with only homogeneously distributed background sources. By investigating a scenario with Centaurus A as a single source in combination with the homogeneous background, we confirm that this region of the sky provides the dominant contribution to the observed anisotropy signal. Models containing a catalog of jetted active galactic nuclei whose flux scales with the gamma-ray emission are, however, disfavored as they cannot adequately describe the measured arrival directions.

JOURNAL OF COSMOLOGY AND ASTROPARTICLE PHYSICS [1], 022, 2024. DOI: 10.1088/1475-7516/2024/01/022

[P023-2024] "Cosmological shocks around galaxy clusters: a coherent investigation with DES, SPT, and ACT"

Anbajagane, D.; Chang, C.; Baxter, E. J.; **Navarro-Alsina, A.*;** et al.

We search for signatures of cosmological shocks in gas pressure profiles of galaxy clusters using the cluster catalogues from three surveys: the Dark Energy Survey (DES) Year 3, the South Pole Telescope (SPT) SZ survey, and the Atacama Cosmology Telescope (ACT) data releases 4, 5, and 6, and using thermal Sunyaev-Zeldovich (SZ) maps from SPT and ACT. The combined cluster sample contains around 10(5) clusters with mass and redshift ranges 10(13.7) < M-200m/ M-circle dot < 10(15.5) and 0.1 < z < 2, and the total sky coverage of the maps is approximate to 15 000 deg(2). We find a clear pressure deficit at R/R-200m approximate to 1.1 in SZ profiles around both ACT and SPT clusters, estimated at 6 sigma significance, which is qualitatively consistent with a shock-induced thermal non-equilibrium between electrons and ions. The feature is not as clearly determined in profiles around DES clusters. We verify that measurements using SPT or ACT maps are consistent across all scales, including in the deficit feature. The SZ profiles of optically selected and SZ-selected clusters are also consistent for higher mass clusters. Those of less massive, optically selected clusters are suppressed on small scales by factors of 2-5 compared to predictions, and we discuss possible interpretations of this behaviour. An oriented stacking of clusters - where the orientation is inferred from the SZ image, the brightest cluster galaxy, or the surrounding large-scale structure measured using galaxy catalogues - shows the normalization of the one-halo and two-halo terms vary with orientation. Finally, the location of the pressure deficit feature is statistically consistent with existing estimates of the splashback radius.

MONTHLY NOTICES OF THE ROYAL ASTRONOMICAL SOCIETY 527[3], 9378-9404, 2024. DOI: 10.1093/mnras/stad3726

[P024-2024] "Disentangling the Effects of Laser and Electron Irradiation on AgX (X = Cl, Br, and I): Insights from Quantum Chemical Calculations"

Cabral, L.*; Leite, E. R.; Longo, E.; San-Miguel, M. A.; **Silva, E. Z. da***; Andrés, J.

The effects on the lattice structure and electronic properties of different polymorphs of silver halide, AgX (X = Cl, Br, and I), induced by laser irradiation (LI) and electron irradiation (EI) are investigated using a first-principles approach, based on the electronic temperature (T-e) within a two-temperature model (TTM) and by increasing the total number of electrons (N-e), respectively. Ab initio molecular dynamics (AIMD) simulations provide a clear visualization of how T-e and N-e induce a structural and electronic transformation process during LI/EI. Our results reveal the diffusion processes of Ag and X ions, the amorphization of the AgX lattices, and a straightforward interpretation of the time evolution for the formation of Ag and X nanoclusters under high values of T-e and N-e. Overall, the present work provides fine details of the underlying mechanism of LI/EI and promises to be a powerful toolbox for further cross-scale modeling of other semiconductors.

NANO LETTERS 24[10], 3021-3027, 2024. DOI: 10.1021/acs.nanolett.3c04130 **(Artigo destaque de capa)**

[P025-2024] "DUNE potential as a new physics probe"

Cherchiglia, A.*; Santiago, J.

Neutrino experiments, in the next years, aim to determine with precision all the six parameters of the three-neutrino standard paradigm. The complete success of the experimental program is, nevertheless, attached to the non-existence (or at least smallness) of Non-Standard Interactions (NSI). In this work, anticipating the data taken from long-baseline neutrino experiments, we map all the weakly coupled theories that could induce sizable NSI, with the potential to be determined in these experiments, in particular DUNE. Once present constraints from other experiments are taken into account, in particular charged-lepton flavor violation, we find that only models containing leptoquarks (scalar or vector) and/or neutral isosinglet vector bosons are viable. We provide the explicit matching formulas connecting weakly coupled models and NSI, both in propagation and production. Departing from the weakly coupled completion with masses at TeV scale, we also provide a global fit on all NSI for DUNE, finding that NSI smaller than 10-2 cannot be probed even in the best-case scenario.

JOURNAL OF HIGH ENERGY PHYSICS [3], 18, 2024. DOI: 10.1007/JHEP03(2024)018

[P026-2024] "Estimating the volume of correlation sets in causal networks"

Camillo, G.; **Lauand, P.*;** Poderini, D.; **Rabelo, R.***; Chaves, R.

Causal networks beyond that in the paradigmatic Bell's theorem can lead to new kinds and applications of nonclassical behavior. Their study, however, has been hindered by the fact that they define a nonconvex set of correlations and only very incomplete or approximated descriptions have been obtained so far, even for the simplest scenarios. Here we take a different stance on the problem and consider the relative volume of classical or nonclassical correlations a given network gives rise to, considering distances to sets of interest and how they distribute too. Among other results, we show instances where the inflation technique, arguably the most disseminated tool in the community, is unable to detect a significant portion of the nonclassical behaviors, up to three copies of each source, and that a concentration phenomenon of distances happens in one of them. Interestingly, we also show that the use of interventions, a central tool in causal inference, can enhance substantially our ability to witness nonclassicality.

PHYSICAL REVIEW A 109[1], 012220, 2024. DOI: 10.1103/PhysRevA.109.012220

[P027-2024] "Evidence of brain metabolism redistribution from neocortex to primitive brain structures in early acute COVID-19 respiratory syndrome"

Souza, S. P. M.; Colet, N.; Fujiwara, M.; Fernandes, A. P.; Tobar, N.; Dertkigil, S. S. J.; **Takahashi, M. E. S.***; Amorim, B. J.; Silva, L. S.; Yasuda, C. L.; Cendes, F.; Souza, T. F. de; Rodrigues, J. T.; Zantut-Wittmann, D. E.; Ramos, C. D.

Background Neuropsychiatric sequelae of COVID-19 have been widely documented in patients with severe neurological symptoms during the chronic or subacute phase of the disease. However, it remains unclear whether subclinical changes in brain metabolism can occur early in the acute phase of the disease. The aim of this study was to identify and quantify changes in brain metabolism in patients hospitalized for acute respiratory syndrome due to COVID-19 with no or mild neurological symptoms. Results Twenty-three non-intubated patients (13 women; mean age 55.5 +/- 12.1 years) hospitalized with positive nasopharyngeal swab test (RT-PCR) for COVID-19, requiring supplemental oxygen and no or mild neurological symptoms were studied. Serum C-reactive protein measured at admission ranged from 6.43 to 189.0 mg/L (mean: 96.9 +/- 54.2 mg/L). The mean supplemental oxygen demand was 2.9 +/- 1.4 L/min. [F-18]FDG PET/CT images were acquired with a median of 12 (4-20) days of symptoms. After visual interpretation of the images, semiquantitative analysis of [F-18]FDG uptake in multiple brain regions was evaluated using dedicated software and the standard deviation (SD) of brain uptake in each region was automatically calculated in comparison with reference values of a normal database. Evolutionarily ancient structures showed positive SD mean values of [F-18]FDG uptake. Lenticular nuclei were bilaterally hypermetabolic (> 2 SD) in 21/23 (91.3%) patients, and thalamus in 16/23 (69.6%), bilaterally in 11/23 (47.8%). About half of patients showed hypermetabolism in brainstems, 40% in hippocampi, and 30% in cerebellums. In contrast, neocortical regions (frontal, parietal, temporal and occipital lobes) presented negative SD mean values of [F-18]FDG uptake and hypometabolism (< 2 SD) was observed in up to a third of patients. Associations were found between hypoxia, inflammation, coagulation markers, and [F-18]FDG uptake in various brain structures. Conclusions Brain metabolism is clearly affected during the acute phase of COVID-19 respiratory syndrome in neurologically asymptomatic or oligosymptomatic patients. The most frequent finding is marked hypermetabolism in evolutionary ancient structures such as lenticular nucleus and thalami. Neocortical metabolism was reduced in up to one third of patients, suggesting a redistribution of brain metabolism from the neocortex to evolutionary ancient brain structures in these patients.

EJNMMI RESEARCH 14[1], 28, 2024. DOI: 10.1186/s13550-024-01089-3

[P028-2024] "Examining the self-interaction of dark matter through central cluster galaxy offsets"

Cross, D.; Thoron, G.; **Sobreira, F.***; et al.
DES Collaboration

While collisionless cold dark matter models have been largely successful in explaining a wide range of observational data, some tensions still exist, and it remains possible that dark matter possesses a non-negligible level of self interactions. In this paper, we investigate a possible observable consequence of self-interacting dark matter: offsets between the central galaxy and the center of mass of its parent halo. We examine 23 relaxed galaxy clusters in a redshift range of 0.1 - 0.3 drawn from clusters in the Dark Energy Survey and the Sloan Digital Sky Survey which have archival Chandra X--ray data of sufficient depth for center and relaxation determination. We find that most clusters in our sample show non-zero offsets between the X-ray center, taken to be the centroid within the cluster core, and the central galaxy position. All of the measured offsets are larger, typically by an order of magnitude, than the uncertainty in the X-ray position due to Poisson noise. In all but six clusters, the measured offsets are also larger than the estimated, combined astrometric uncertainties in the X-ray and optical positions. A more conservative cut on concentration to select relaxed clusters marginally reduces but does not eliminate the observed offset. With our more conservative sample, we find an estimated mean X-ray to central galaxy offset of mu=6.0(-1.5)(+1.4)kpc. Comparing to recent simulations, this distribution of offsets is consistent with some level of dark matter self interaction, though further simulation work is needed to place constraints.

MONTHLY NOTICES OF THE ROYAL ASTRONOMICAL SOCIETY 529[1], 52-58, 2024. DOI: 10.1093/mnras/stae442

[P029-2024] "Exploring the phase diagrams of multidimensional Kuramoto models"

Fariello, R.; **Aguiar, M. A. M. de***

The multidimensional Kuramoto model describes the synchronization dynamics of particles moving on the surface of -dimensional spheres, generalizing the original model where they are characterized by a single phase. Particles are represented by -dimensional unit vectors and the coupling constant can be extended to a coupling matrix acting on the vectors. The system has a large number of independent parameters, given by the characteristic widths of the distributions of natural frequencies and the entries of the coupling matrix. Moreover, as the coupling matrix breaks the rotational symmetry, the average values of the natural frequencies also play a key role in the dynamics. General phase diagrams, indicating regions in parameter space where the system exhibits different behaviors, are hard to derive analytically. Here we obtain the complete phase diagram for, for arbitrary coupling matrice and Lorentzian distributions of natural frequencies. We show that the system exhibits four different phases: disordered and static synchrony (as in the original Kuramoto model), rotation of the synchronized cluster (similar to the Kuramoto-Sakaguchi model with frustration) and active synchrony, a new phase where the module of the order parameter oscillates as it rotates on the sphere. We also explore the diagrams numerically for higher dimensions, and, for particular choices of coupling matrices and frequency distributions. We find that the system always exhibits the same four phases, but their location in the space of parameters depends strongly on the dimension being even or odd, on the coupling matrix and on the shape of the distribution of natural frequencies

CHAOS SOLITONS & FRACTALS 179, 114431, 2024. DOI: 10.1016/j.chaos.2023.114431

[P030-2024] "Green Fabrication and Analytical Application of Disposable Carbon Electrodes Made from Fallen Tree Leaves Using a CO2 Laser"

Blasques, R. V.; Camargo, J. R.; Veloso, W. B.; Meloni, G. N.; Fernandes, F. A.; Germinare, B. F.; Silva, L. R. G. e; **Siervo, A. de***; Paixao, T. R. L. C.; Janegitz, B. C.

The use of materials from nature to prepare sensors is a challenge, once we can generate great value with respect to the environment. In this regard, the carbonization of several types of substrates through the utilization of a CO2 laser promotes the fabrication of exceptional electrochemical sensors that exhibit different architectures, all while adhering to the principles of eco-friendliness and cost-efficiency. In this context, the pursuit of novel substrates derived from renewable sources, characterized by their accessibility and wide availability, is important in the advancement of cutting-edge electrochemical sensors. In this scenario, the study into the utilization of fallen tree leaves is presented for the first time, capitalizing on the pyrolytic transformation induced by a CO2 laser, to fabricate electrochemical sensors. During the sensor fabrication process, the parameters of the CO2 laser, including laser power, pyrolysis scan rate, and scan gap, are systematically adjusted to attain optimal outcomes. The proposed sensors were characterized through electrochemical, morphological, and physicochemical methodologies, thereby enabling an exhaustive exploration of the novel carbonized surface generated on the leaves. Also, to underscore the applicability of the sensors, they have been employed in the detection of dopamine and paracetamol in biological and pharmaceutical samples. The applications of this system show a linear range of 10-1200 mu mol L-1 for dopamine and 5.0-100.0 mu mol L-1 for paracetamol, with limits of detection of 1.1 and 0.76 mu mol L-1, respectively. In this manner, electrochemical sensors derived from fallen tree leaves exhibit satisfactory analytical performance and remarkable reproducibility, thus highlighting their substantial potential to replace conventional substrates.

ACS SUSTAINABLE CHEMISTRY & ENGINEERING 12[8], 3061-3072, 2024. DOI: 10.1021/acssuschemeng.3c06526

[P031-2024] "High precision orientation mapping from 4D--STEM precession electron diffraction data through quantitative analysis of diffracted intensities"

Corrêa, L. M.*; Ortega, E.; Ponce, A.; **Cotta, M. A.*; Ugarte, D.***

The association of scanning transmission electron microscopy (STEM) and detection of a diffraction pattern at each probe position (so-called 4D-STEM) represents one of the most promising approaches to analyze structural properties of materials with nanometric resolution and low irradiation levels. This is widely used for texture analysis of materials using automated crystal orientation mapping (ACOM). Herein, we perform orientation mapping in InP nanowires exploiting precession electron diffraction (PED) patterns acquired by an axial CMOS camera.Crystal orientation is determined at each probe position by the quantitative analysis of diffracted intensities minimizing a residue comparing experiments and simulations in analogy to x-ray structural refinement. Our simulations are based on the two-beam dynamical diffraction approximation and yield a high angular precision (-0.03 degrees), much lower than the traditional ACOM based on pattern matching algorithms (-1 degrees). We anticipate that simultaneous exploration of both spot positions and high precision crystal misorientation will allow the exploration of the whole potentiality provided by PED-based 4D-STEM for the characterization of deformation fields in nanomaterials.

ULTRAMICROSCOPY 259, 113927, 2024. DOI: 10.1016/j.ultramic.2024.113927

[P032-2024] "Influence of terephthalate anion in ZnAl layered double hydroxide on lead ion removal: Adsorption, kinetics, thermodynamics and mechanism"

Aquino, R. V. S. de; Lucena, P. G. C. de; Arias, S.; **Landers, R.***; Pacheco, J. G. A.; Rocha, O. R. Sa da

In this work, layered double hydroxides (LDHs) intercalated with carbonate (ZnAl-CO3) and terephthalate (ZnAl-TA) anions were synthesized for the removal of lead (Pb2+) ions from aqueous solutions. ZnAl-TA showed better Pb2+ removal performance than ZnAl-CO3. In the kinetic study, the Elovich model obtained the best fit; the Weber-Morris model showed that intraparticle diffusion is not a limiting step in the process. The Sips model fitted better to the adsorption isotherms, with a maximum adsorption capacity of 124 mg.g(-1). The thermodynamic study showed that the process is spontaneous and endothermic. In the regeneration of ZnAl--TA, the use of NaCl as a desorption eluent showed less Zn2+ leaching and greater desorption efficiency compared to acid eluents. The adsorption capacity of Pb2+ in the presence of other ions followed the order Ni2+ > Ca2+ > Cd2+ > Mg2+ > Cu2+. The ZnAl-TA adsorbent reached 88% of its initial efficiency after 3 cycles with high stability. From post-adsorption XRD, FTIR, and XPS analyses, Pb2+ was removed predominantly by chelation, surface complexation, and precipitation. In general, the ZnAl-TA adsorbent proved to be an efficient sorbent material for Pb2+ removal from aqueous effluent.

COLLOIDS AND SURFACES A-PHYSICOCHEMICAL AND ENGINEERING ASPECTS 686, 133404, 2024. DOI: 10.1016/j.colsurfa.2024.133404

[P033-2024] "Light, Copper, Action: Visible-Light Illumination Enhances Bactericidal Activity of Copper Particles"

Schio, A. L.; Lima, M. S. de; Frassini, R.; Scariot, F. J.; **Cemin, F.***; Elois, M. A.; **Alvarez, F.***; Michels, A. F.; Fongaro, G.; Roesch-Ely, M.; Figueroa, C. A.

Bacteria are an old concern to human health, as they are responsible for nosocomial infections, and the number of antibiotic-resistant microorganisms keeps growing. Copper is known for its intrinsic biocidal properties, and therefore, it is a promising material to combat infections when added to surfaces. However, its biocidal properties in the presence of light illumination have not been fully explored, especially regarding the use of microsized particles since nanoparticles have taken over all fields of research and subjugated microparticles despite them being abundant and less expensive. Thus, the present work studied the bactericidal properties of metallic copper particles, in microscale (CuMPs) and nanoscale (CuNPs), in the absence of light and under white LED light illumination.The minimum bactericidal concentration (MBC) of CuMPs against Staphylococcus aureus that achieved a 6-log reduction was 5.0 and 2.5 mg mL(-1) for assays conducted in the absence of light and under light illumination, respectively. Similar behavior was observed against Escherichia coli. The bactericidal activity under illumination provided a percentage increase in log reduction values of 65.2% for S. aureus and 166.7% for E. coli when compared to the assays under dark. This assay reproduced the testing CuNPs, which showed superior bactericidal activity since the concentration of 2.5 mg mL(-1) promoted a 6-log reduction of both bacteria even under dark.Its superior bactericidal activity, which overcame the effect of illumination, was expected once the nanoscale facilitated the interaction of copper within the surface of bacteria.

The results from MBC were supported by fluorescence microscopy and atomic absorption spectroscopy. Therefore, CuMPs and CuNPs proved to have size- and dose-dependent biocidal activity. However, we have shown that CuMPs photoactivity is competitive compared to that of CuNPs, allowing their application as a self-cleaning material for disinfection processes assisted by conventional light sources without additives to contain the spread of pathogens.

ACS BIOMATERIALS SCIENCE & ENGINEERING, 2024. DOI: 10.1021/acsbiomaterials.3c01873. Early Access Date: FEB 2024

[P034-2024] "Measurement of the Higgs boson production via vector boson fusion and its decay into bottom quarks in proton-proton collisions at √s=13 TeV"

Hayrapetyan, A.; Tumasyan, A.; **Chinellato, J. A.***; et al.
CMS Collaboration

A measurement of the Higgs boson (H) production via vector boson fusion (VBF) and its decay into a bottom quark-antiquark pair (b (b) over bar) is presented using proton-proton collision data recorded by the CMS experiment at root s = 13TeV and corresponding to an integrated luminosity of 90.8 fb(-1). Treating the gluon-gluon fusion process as a background and constraining its rate to the value expected in the standard model (SM) within uncertainties, the signal strength of the VBF process, defined as the ratio of the observed signal rate to that predicted by the SM, is measured to be mu(qqH)(Hb (b) over bar) = 1.01(-0.46)(+0.55). The VBF signal is observed with a significance of 2.4 standard deviations relative to the background prediction, while the expected significance is 2.7 standard deviations. Considering inclusive Higgs boson production and decay into bottom quarks, the signal strength is measured to be mu(incl.) (Hb (b) over bar) = 0.99(-0.41)(+0.48), corresponding to an observed (expected) significance of 2.6 (2.9) standard deviations.

JOURNAL OF HIGH ENERGY PHYSICS [1], 173, 2024. DOI: 10.1007/JHEP01(2024)173

[P035-2024] "Measurement of the radius dependence of charged-particle jet suppression in Pb-Pb collisions at √SNN=5.02 TeV"

Acharya, S.; Adamova, D.; **Chinellato, D. D.*; Guardiano, G. G.*; Jahnke, C.*; Takahashi, J.***; et al.
ALICE Collaboration

The ALICE Collaboration reports a differential measurement of inclusive jet suppression using pp and Pb-Pb collision data at a center -of -mass energy per nucleon-nucleon collision root SNN = 5.02 TeV. Charged -particle jets are reconstructed using the anti-kT algorithm with resolution parameters R = 0.2, 0.3, 0.4, 0.5, and 0.6 in pp collisions and R = 0.2, 0.4, 0.6 in central (0-10%), semi -central (30-50%), and peripheral (60-80%) Pb-Pb collisions. A novel approach based on machine learning is employed to mitigate the influence of jet background. This enables measurements of inclusive jet suppression in new regions of phase space, including down to the lowest jet pT >= 40 GeV/c at R = 0.6 in central Pb-Pb collisions. This is an important step for discriminating different models of jet quenching in the quark-gluon plasma. The transverse momentum spectra, nuclear modification factors, derived cross section, and nuclear modification factor ratios for different jet resolution parameters of charged -particle jets are presented and compared to model predictions. A mild dependence of the nuclear modification factor ratios on collision centrality and resolution parameter is observed. The results are compared to a variety of jet -quenching models with varying levels of agreement.

PHYSICS LETTERS B 849, 138412, 2024. DOI: 10.1016/j.physletb.2023.138412

[P036-2024] "Measurements of inclusive J/ψ production at midrapidity and forward rapidity in Pb-Pb collisions at √sNN=5.02 TeV"

Acharya, S.; Adamova, D.; **Chinellato, D. D.*; Guardiano, G. G.*; Jahnke, C.*; Liveraro, G. S. S.*; Takahashi, J.***; et al.
ALICE Collaboration

The measurements of the inclusive J/psi yield at midrapidity (|y| < 0.9) and forward rapidity (2.5 < y < 4) in Pb-Pb collisions at root s(NN) = 5.02 TeV with the ALICE detector at the LHC are reported. The inclusive J/psi production yields and nuclear modification factors, R-AA, are measured as a function of the collision centrality, J/psi transverse momentum (p(T)), and rapidity. The J/psi average transverse momentum and squared transverse momentum (< p(T)> and < p(T)(2)>) are evaluated as a function of the centrality at midrapidity. Compared to the previous ALICE publications, here the entire Pb-Pb collisions dataset collected during the LHC Run 2 is used, which improves the precision of the measurements and extends the p(T) coverage. The p(T)-integrated R-AA shows a hint of an increasing trend towards unity from semicentral to central collisions at midrapidity, while it is flat at forward rapidity. The p(T)-differential R-AA shows a strong suppression at high p(T) with less suppression at low p(T) where it reaches a larger value at midrapidity compared to forward rapidity. The ratio of the p(T)-integrated yields of J/psi to those of D-0 mesons is reported for the first time for the central and semicentral event classes at midrapidity. Model calculations implementing charmonium production via the coalescence of charm quarks and antiquarks during the fireball evolution (transport models) or in a statistical approach with thermal weights are in good agreement with the data at low p(T). At higher p(T), the data are well described by transport models and a model based on energy loss in the strongly-interacting medium produced in nuclear collisions at the LHC.

PHYSICS LETTERS B 849, 138451, 2024. DOI: 10.1016/j.physletb.2024.138451

[P037-2024] "Measurements of long-range two-particle correlation over a wide pseudorapidity range in p-Pb collisions at √sNN=5.02 TeV"

Acharya, S.; Adamova, D.; **Chinellato, D. D.*; Guardiano, G. G.*; Liveraro, G. S. S.*; Takahashi, J.*;** et al.
ALICE Collaboration

Correlations in azimuthal angle extending over a long range in pseudorapidity between particles, usually called the "ridge" phenomenon, were discovered in heavy-ion collisions, and later found in pp and p-Pb collisions. In large systems, they are thought to arise from the expansion (collective flow) of the produced particles. Extending these measurements over a wider range in pseudorapidity and final-state particle multiplicity is important to understand better the origin of these long-range correlations in small collision systems. In this Letter, measurements of the long-range correlations in p-Pb collisions at root s(NN) = 5.02 TeV are extended to a pseudorapidity gap of Delta eta similar to 8 between particles using the ALICE forward multiplicity detectors. After suppressing non--flow correlations, e.g., from jet and resonance decays, the ridge structure is observed to persist up to a very large gap of Delta eta similar to 8 for the first time in p-Pb collisions. This shows that the collective flow-like correlations extend over an extensive pseudorapidity range also in small collision systems such as p-Pb collisions. The pseudorapidity dependence of the second-order anisotropic flow coefficient, v(2)(eta), is extracted from the long-range correlations. The v(2)(eta) results are presented for a wide pseudorapidity range of -3.1 < eta < 4.8 in various centrality classes in p-Pb collisions. To gain a comprehensive understanding of the source of anisotropic flow in small collision systems, the v(2)(eta) measurements are compared with hydrodynamic and transport model calculations.

The comparison suggests that the final-state interactions play a dominant role in developing the anisotropic flow in small collision systems.

JOURNAL OF HIGH ENERGY PHYSICS [1], 199, 2024. DOI: 10.1007/JHEP01(2024)199

[P038-2024] "Modeling 4HeN Clusters with Wave Functions Based on Neural Networks"

Freitas, W.*; Abreu, B.; **Vitiello, S. A.***

A recently introduced neural network-based trial wave function, in combination with the variational Monte Carlo method, is applied to clusters of helium atoms of several sizes. Energies of clusters ranging from 11 to 24 atoms and radial distribution functions are reported in excellent agreement with those of the droplet model obtained with diffusion Monte Carlo. The abilities of neural networks to recognize patterns and relationships from distinct input features are explored, including identifying radial symmetry without explicitly considering it in the network inputs. The relation between data representation and the learning process is investigated, showing that high-quality data representations are critical for the efficient use of neural networks.

JOURNAL OF LOW TEMPERATURE PHYSICS, 2024. DOI: 10.1007/s10909-024-03061-w. Early Access Date: MAR 2024

[P039-2024] "Motor Imagery Neurofeedback: From System Conceptualization to Neural Correlates"

Stefano Filho, C. A.*; Attux, R.; **Castellano, G.***

Purpose of ReviewAs a topic review on neurofeedback and motor imagery, this work revises the overall foundations and conceptualization of neurofeedback training (NFBT), focusing on its current trends and applications in the field of motor imagery (MI). This paradigm consists of imagined execution of motor action, without the explicit motor output and has potential beneficial applications in motor rehabilitation protocols. Given the complexity of MI, aiming to also provide an entry-level basis in the subject, we have compiled basic aspects of movement execution as well, to support better understanding of the covert aspects of the processes involved in its planning stages.Recent FindingsWe have explored recent trends regarding the individualization of MI protocols for NFBT and brain-computer interfaces, which seems to be an emerging branch of evaluations in the field. After establishing a fundamental basis on motor functions, the conceptualization of MI is explored through the contrast of the cognitive and motor models for explaining the task. Research evidence for both models are discussed through reviewing the main areas involved, as revealed by functional neuroimaging studies. SummaryFinally, we discuss recent trends in NFBT-MI practice.

CURRENT BEHAVIORAL NEUROSCIENCE REPORTS, 2024. DOI: 10.1007/s40473-024-00275-w. Early Access Date: FEB 2024

[P040-2024] "On the physical meaning of the geometric factor and the effective thickness in the Montgomery method"

Oliveira, F. S.*; Alves, L. M. S.; Luz, M. S. da; Romao, E. C.; Santos, C. A. M. dos

The Montgomery method is extensively employed to determine the electrical resistance tensor of anisotropic samples. This technique relies on two essential parameters describing an isotropic system: the geometric factor (H1) and the effective thickness (E). The numerical values of these parameters are intricately linked to the dimensions of an isotropic block equivalent to the studied anisotropic specimen. While these parameters hold importance, the physical interpretation of these terms still lacks clarity. In this study, we utilized the finite element method to simulate electrical transport experiments across samples of various shapes. Utilizing the Electric Currents physics interface in the COMSOL program, we were able to provide a comprehensive analysis of the physical meaning of these parameters to accurately determine the electrical properties of thin films and wafers. The presented findings related to the physical interpretation of H1 and E terms make substantial contributions to the field of electrical transport experimental techniques, which are fundamental to design advanced materials for technological applications and understand their physical properties.

AIP ADVANCES 14[2], 025036, 2024. DOI: 10.1063/5.0156453

[P041-2024] "Parity violation in resonant inelastic soft x--ray scattering at entangled core holes"

Soederstroem, J.; Ghosh, A.; Kjellsson, L.; Ekholm, V.; Tokushima, T.; Såthe, C.; Velasquez, N.; Simon, M.; Björneholm, O.; Duda, L.; **Brito, A. N. de***; Odelius, M.; Liu, J. C.; Wang, J.; Kimberg, V.; Agåker, M.; Rubensson, J. E.; Gel'mukhanov, F.

Resonant inelastic x-ray scattering (RIXS) is a major method for investigation of electronic structure and dynamics, with applications ranging from basic atomic physics to materials science. In RIXS applied to inversion-symmetric systems, it has generally been accepted that strict parity selectivity applies in the sub-kilo-electron volt region. In contrast, we show that the parity selection rule is violated in the RIXS spectra of the free homonuclear diatomic O-2 molecule. By analyzing the spectral dependence on scattering angle, we demonstrate that the violation is due to the phase difference in coherent scattering at the two atomic sites, in analogy with Young's double-slit experiment. The result also implies that the interpretation of x-ray absorption spectra for inversion symmetric molecules in this energy range must be revised.

SCIENCE ADVANCES 10[7], eadk3114, 2024. DOI: 10.1126/sciadv.adk3114

[P042-2024] "Prompt and non-prompt J/ψ production at midrapidity in Pb-Pb collisions at √sNN=5.02 TeV"

Acharya, S.; Adamová, D.; **Chinellato, D. D.*; Guardiano, G. G.*; Liveraro, G. S. S.*; Takahashi, J.***; et al.
ALICE Collaboration

The transverse momentum (p(T)) and centrality dependence of the nuclear modification factor R-AA of prompt and non-prompt J/psi, the latter originating from the weak decays of beauty hadrons, have been measured by the ALICE collaboration in Pb-Pb collisions at root s(NN) = 5.02TeV. The measurements are carried out through the e(+)e(-) decay channel at midrapidity (vertical bar y vertical bar < 0.9) in the transverse momentum region 1.5 < p(T) < 10 GeV/c. Both prompt and non-prompt J/psi measurements indicate a significant suppression for p(T) > 5 GeV/c, which becomes stronger with increasing collision centrality. The results are consistent with similar LHC measurements in the overlapping pT intervals, and cover the kinematic region down to p(T) = 1.5 GeV/c at midrapidity, not accessible by other LHC experiments. The suppression of prompt J/psi in central and semicentral collisions exhibits a decreasing trend towards lower transverse momentum, described within uncertainties by models implementing J/psi production from recombination of c and (c) over bar quarks produced independently in different partonic scatterings. At high transverse momentum, transport models including quarkonium dissociation are able to describe the suppression for prompt J/psi. For non--prompt J/psi, the suppression predicted by models including

both collisional and radiative processes for the computation of the beauty-quark energy loss inside the quark-gluon plasma is consistent with measurements within uncertainties.

JOURNAL OF HIGH ENERGY PHYSICS [2], 066, 2024. DOI: 10.1007/JHEP02(2024)066

[P043-2024] "Radio measurements of the depth of air-shower maximum at the Pierre Auger Observatory"

Halim, A. A.; Abreu, P.; **Bonneau Arbeletche, L.*; Chinellato, J. A.*; Oliveira Franco, D.*; Dobrigkeit, C.*; Fauth, A. C.*; Machado Payeras, A.*; Reginatto Akim, J. V.***; et al.
Pierre Auger Collaboration

The Auger Engineering Radio Array (AERA), part of the Pierre Auger Observatory, is currently the largest array of radio antenna stations deployed for the detection of cosmic rays, spanning an area of 17 km2 with 153 radio stations. It detects the radio emission of extensive air showers produced by cosmic rays in the 30-80 MHz band. Here, we report the AERA measurements of the depth of the shower maximum (Xmax), a probe for mass composition, at cosmic-ray energies between 1017.5 and 1018.8 eV, which show agreement with earlier measurements with the fluorescence technique at the Pierre Auger Observatory. We show advancements in the method for radio Xmax reconstruction by comparison to dedicated sets of CORSIKA/COREAS air-shower simulations, including steps of reconstruction-bias identification and correction, which is of particular importance for irregular or sparse radio arrays. Using the largest set of radio air-shower measurements to date, we show the radio Xmaxresolution as a function of energy, reaching a resolution better than 15 g cm-2 at the highest energies, demonstrating that radio Xmax measurements are competitive with the established high-precision fluorescence technique. In addition, we developed a procedure for performing an extensive data-driven study of systematic uncertainties, including the effects of acceptance bias, reconstruction bias, and the investigation of possible residual biases. These results have been cross-checked with air showers measured independently with both the radio and fluorescence techniques, a setup unique to the Pierre Auger Observatory.

PHYSICAL REVIEW D 109[2], 022002, 2024. DOI: 10.1103/PhysRevD.109.022002

[P044-2024] "Reproducibility of arterial spin labeling cerebral blood flow image processing: A report of the ISMRM open science initiative for perfusion imaging (OSIPI)_and the ASL MRI challenge"

Paschoal, A. M.*; Woods, J. G.; Pinto, J.; Bron, E. E.; Petr, J.; McConnell, F. A. K.; Bell, L.; Dounavi, M. E.; van Praag, C. G.; Mutsaerts, H. J. M. M.; Taylor, A. O.; Zhao, M. Y.; Brumer, I.; Chan, W. S. M.; Toner, J.; Hu, J.; Zhang, L. X.; Domingos, C.; Monteiro, S. P.; Figueiredo, P.; Harms, A. G. J.; Padrela, B. E.; Tham, C.; Abdalle, A.; Croal, P. L.; Anazodo, U.

Purpose: Arterial spin labeling (ASL) is a widely used contrast-free MRI method for assessing cerebral blood flow (CBF). Despite the generally adopted ASL acquisition guidelines, there is still wide variability in ASL analysis. We explored this variability through the ISMRM-OSIPI ASL-MRI Challenge, aiming to establish best practices for more reproducible ASL analysis. Methods: Eight teams analyzed the challenge data, which included a high-resolution T1-weighted anatomical image and 10 pseudo-continuous ASL datasets simulated using a digital reference object to generate ground-truth CBF values in normal and pathological states.We compared the accuracy of CBF quantification from each team's analysis to the ground truth across all voxels and within predefined brain regions. Reproducibility of CBF across analysis pipelines was assessedusing the intra-class correlation coefficient (ICC), limits of agreement (LOA), and replicability of generating similar CBF estimates from different processing approaches. Results: Absolute errors in CBF estimates compared to ground-truth synthetic data ranged from 18.36 to 48.12 mL/100 g/min. Realistic motion incorporated into three datasets produced the largest absolute error and variability between teams, with the least agreement (ICC and LOA) with ground-truth results. Fifty percent of the submissions were replicated, and one produced three times larger CBF errors (46.59 mL/100 g/min) compared to submitted results. Conclusions: Variability in CBF measurements, influenced by differences in image processing, especially to compensate for motion, highlights the significance of standardizing ASL analysis workflows. We provide a recommendation for ASL processing based on top-performing approaches as a step toward ASL standardization.

MAGNETIC RESONANCE IN MEDICINE, 2024. DOI: 10.1002/mrm.30081 Early Access Date: MAR 2024

[P045-2024] "Resistance training effects on pubertal children with a risk of developing pediatric dynapenia"

Ruas, C. V.*; Ratel, S.; Nosaka, K.; **Castellano, G.***; Pinto, R. S.

Purpose Many modern-day children are at risk of pediatric dynapenia (muscle weakness). We examined the effects of a 12-week resistance training (RT) program on neuromuscular function and body composition parameters in pubertal children with a risk of dynapenia. Methods Twelve children (13.4 +/- 0.9 y) with dynapenia performed a progressive RT program consisting of knee extension and flexion, bench press, abdominal crunch, back extension, lateral pull-down, elbow flexion, and upright row (1-2 sets of 10-15 repetitions/exercise) twice/week for 12 weeks. Outcome measures included one-repetition maximum (1-RM) strength, maximal voluntary isometric contraction (MVIC) torque, rate of torque development (RTD), electromyographic (EMG) activity, muscle thickness (MT), muscle quality (MQ) assessed by echo intensity (MQ(EI)) of the knee extensors and specific tension of MVIC torque to thigh fat-free mass (MQ(ST)), and total and regional body and bone composition assessed by dual-energy X-ray absorptiometry. Changes in the measures before and after the 12-week RT and associations among the measures were analyzed by linear mixed models. Results Significant ($p < 0.05$) increases in 1-RM (63.9 +/- 4.5%), MVIC torque (16.3 +/- 17.8%), MT (18.8 +/- 5.5%) and MQ (MQ(EI): -25.9 +/- 15.2%; MQ(ST): 15.1 +/- 18.8%;) were evident from pre- to post-training. Total fat-free mass (FFM) increased by 2.3 +/- 3.2% from baseline ($p = 0.01$), but no changes ($p > 0.05$) in the other measures were observed. Significant ($p < 0.05$) associations between the changes in 1-RM and/or MVIC torque and the changes in quadriceps MT, MQ(EI), MQ(ST) and total body FFM were evident. Conclusions The 12-week RT was effective for improving neuromuscular and body composition parameters, and thereby reversed the risk of pediatric dynapenia.

EUROPEAN JOURNAL OF APPLIED PHYSIOLOGY, 2024. DOI: 10.1007/s00421-024-05436-z. **Early Access Date:** FEB 2024

[P046-2024] "Resonances of Supernova Neutrinos in Twisting Magnetic Fields"

Jana, S.; **Porto, Y.***

We investigate the effect of resonant spin conversion of the neutrinos induced by the geometrical phase in a twisting magnetic field. We find that the geometrical phase originating from the rotation of the transverse magnetic field along the neutrino trajectory can trigger a resonant spin conversion of Dirac neutrinos inside the supernova, even if there were no such transitions in the fixed-direction field case. We have shown that, even though resonant spin conversion is too weak to affect solar neutrinos, it could have a remarkable consequence on supernova neutronization bursts where very intense magnetic fields are quite likely.

We demonstrate how the flavor composition at Earth can be used as a probe to establish the presence of non-negligible magnetic moments, potentially down to 10-15 mu B in upcoming neutrino experiments like the Deep Underground Neutrino Experiment and the Hyper-Kamiokande. Possible implications are analyzed.

PHYSICAL REVIEW LETTERS 132[10], 101005, 2024. DOI: 10.1103/PhysRevLett.132.101005

[P047-2024] "Reversible actuation of α-borophene nanoscrolls"

Fabris, G. S. L.; **Galvao, D. S.***; Paupitz, R.

In this work, we proposed and investigated the structural and electronic properties of boron-based nanoscrolls (armchair and zigzag) using the DFTB+ method. We also investigated the electroactuation process (injecting and removing charges). A giant electroactuation was observed, but the results show relevant differences between the borophene and carbon nanoscrolls. The molecular dynamics simulations showed that the scrolls are thermally and structurally stable for a large range of temperatures (up to 600 K), and the electroactuation process can be easily tuned and can be entirely reversible for some configurations. DFT-based simulations are used to investigate the possible existence of boron nanoscrolls, which are shown to be thermally stable and to present a giant and reversible electroactuation.

PHYSICAL CHEMISTRY CHEMICAL PHYSICS, 2024. DOI: 10.1039/d3cp06193k. Early Access Date: MAR 2024

[P048-2024] "Solid State Reaction Epitaxy, A New Approach for Synthesizing Van der Waals heterolayers: The Case of Mn and Cr on Bi2Se3"

Khatun, S.; Alanwoko, O.; Pathirage, V.; Oliveira, C. C. de; **Tromer, R. M.***; Autreto, P. A. S.; **Galvao, D. S.***; Batzill, M.

Van der Waals (vdW) heterostructures that pair materials with diverse properties enable various quantum phenomena. However, the direct growth of vdW heterostructures is challenging. Modification of the surface layer of quantum materials to introduce new properties is an alternative process akin to solid state reaction.Here, vapor deposited transition metals (TMs), Cr and Mn, are reacted with Bi2Se3 with the goal to transform the surface layer to XBi2Se4 (X = Cr, Mn). Experiments and ab initio MD simulations demonstrate that the TMs have a high selenium affinity driving Se diffusion toward the TM. For monolayer Cr, the surface Bi2Se3 is reduced to Bi-2-layer and a stable (pseudo) 2D Cr1+delta Se2 layer is formed. In contrast, monolayer Mn can transform upon mild annealing into MnBi2Se4. This phase only forms for a precise amount of initial Mn deposition. Sub-monolayer amounts dissolve into the bulk, and multilayers form stable MnSe adlayers. This study highlights the delicate energy balance between adlayers and desired surface modified layers that governs the interface reactions and that the formation of stable adlayers can prevent the reaction with the substrate. The success of obtaining MnBi2Se4 points toward an approach for the engineering of other multicomponent vdW materials by surface reactions.
 (TR Abstract Type: graphical; Abstract Language: en) Solid state reaction of Cr and Mn with Bi2Se3 surface is investigated. Cr reacts with Se to form a 2D Cr1+delta Se2 adlayer while reducing Bi2Se3 to Bi-2. In contrast, precisely controlled monolayer amounts of Mn transforms the surface layer to MnBi2Se4. The different interface reactions are due to varying stability of the monolayer selenides and the mixed bismuth selenide phases.

ADVANCED FUNCTIONAL MATERIALS, 2024. DOI: 10.1002/adfm.202315112 Early Access Date: MAR 2024

[P049-2024] "Structural and Magnetic Properties of a Pyridyl(vinyl)benzoate-Based Metal-Organic Framework with Iron(II) as Spin Carrier"

Dezotti, Y.; Vaz, R. C. A.; Ribeiro, M. A.; Passamani, E. C.; **Almeida, A. A. de*; Knobel, M.***; Ardisson, J. D.; Barros, W. P.

The synthesis and structural, magnetic, and hyperfine properties of a new metal-organic framework are presented. Its chemical formula is [Fe-6(pvb)(4)(HCOO)(6)(OH)(2)](n)<middle dot>2n(dmf)<middle dot>2n(H2O) (1), where pvb(-) = bis{4-[2-(4-pyridyl)vinyl]} benzoate. Compound 1 was obtained under hydro(solvo)thermal conditions, presenting a hexanuclear iron(II) motif, which extends through HCOO- and pvb(-) bridges, resulting in a 2D framework linked covalently to adjacent analogous layers by the pvb(-) ligands to form a 3D coordination polymer. 300 and 80 K Fe-57 M & ouml;ssbauer data suggested two paramagnetic iron(II) species in the extended structure of compound 1, presenting a distorted octahedral high-spin state. Alternating current magnetization data recorded in zero and in-field showed two well-defined ordering temperatures at ca. 13 and 2.5 K for the two iron(II) species in less and highly distorted octahedral symmetry, respectively. The system undergoes magnetic transition from a paramagnetic state at high temperatures to a magnetically ordered state at 13 K. At 2.5 K, the ordered spins present a canted-like structure. These magnetic states are field dependent, showing a metamagnetic phase transition for fields higher than 5 kOe. A remnant magnetization of 1.91 N beta and a coercive field, H-C, of 10 kOe are obtained at 2 K, indicating a hard magnetic state often found when AF and FM exchange interactions are present.

CRYSTAL GROWTH & DESIGN, 2024. DOI: 10.1021/acs.cgd.3c01246. Early Access Date: FEB 2024

[P050-2024] "Study of the d-f magnetic interaction in V--doped RCrO4 (RTb, Dy, Er and Yb) compounds"

Jesus, A. C. B.; **Carvalho, M. H.*;** Jesus, J. R.; Mercena, S. G.; **Pagliuso, P. G.*;** Bittar, E. M.; Duque, J. G. S.; Meneses, C. T.

In this work, we have carried out a detailed study of the structural and magnetic properties of RVxCr1-xO4 (R Tb, Dy, Er, and Yb; x = 0.0, 0.3, 0.5, 0.7 and 1.0) compounds obtained by the co-precipitation method. X-ray diffraction data using Rietveld refinement shows that all samples present a single phase consistent with the zircon-type structure (I4(1)/amd space group (No. 141)). The lattice parameter changes as a function of both V-concentration and the rare earth ion. The analyses on T-dependent magnetic susceptibility indicate that RCrO4 samples are ferromagnetic while RVxCr1-xO4 ones are antiferromagnetic for x = 0.7 and 1.0. The increase of magnetic transition temperatures from 3 K (RVO4) to 20 K (RCrO4) can be an indicator that the R-Cr magnetic interaction takes an important role in the magnetic properties in these compounds. Isothermal magnetization curves measured at T = 2 K for all samples reinforce the ferromagnetic character of RCrO4 samples once they present remanence, coercivity, and magnetization saturation. However, the fact that the expected g(J)J value for the full multiplet is not reached for all samples must be associated with the crystal electric field on the rare earth ion.

SOLID STATE SCIENCES 147, 107402, 2024. DOI: 10.1016/j.solidstatesciences.2023.107402

[P051-2024] "Synergy of shaped-induced enhanced Raman scattering to improve surface-enhanced Raman scattering signal in the thiram molecule detection"

Bär, J.; Barros, A. de; **Shimizu, F. M.***; Sigoli, F. A.; Bufon, C. C. B.; Mazali, I. O.

Herein, we explore the combined effect of Shaped-Induced

Enhanced Raman Scattering (SIERS) and SurfaceEnhanced Raman Scattering (SERS) for detecting thiram molecules. We fabricated V-shaped microchannels on a silicon (100) substrate through a standard lithography and etching process. The analysis of SIERS@SERS was performed for Si -V substrates modified with AuNRs with different thiram concentrations, 10-7 to 10-10 mol/L. The spectra were collected for different regions of the Si -V substrates, i.e., in the inside, edge, between (flat top), and far from Si -V (coffee-ring AuNRs aggregation) to assess the performance of Si -V microchannels obtained. The IDMAP statistical projection reveals a higher silhouette coefficient of 0.91 for the inside of Si -V, indicating a more excellent spectral reproducibility with closer relative intensities. The device platform used in this study stands out as a robust option for commercial sensors, demonstrating exceptional sensitivity in detecting a diverse range of molecules, even at low concentrations.

SPECTROCHIMICA ACTA PART A-MOLECULAR AND BIOMOLECULAR SPECTROSCOPY 310, 123907, 2024. DOI: 10.1016/j.saa.2024.123907

[P052-2024] "System-size dependence of the hadronic rescattering effect at energies available at the CERN Large Hadron Collider"

Acharya, S.; Adamova, D.; **Chinellato, D. D.*; Guardiano, G. G.*; Jahnke, C.*; Liveraro, G. S. S.*; Takahashi, J.*;** et al.

The first measurements of K-& lowast;(892)(0)resonance production as a function of charged-particle multiplicity in Xe--Xe collisions at root sNN=5.44 TeV and pp collisions at root s=5.02 TeV using the ALICE detector are presented.The resonance is reconstructed at midrapidity (|y| < 0.5) using the hadronic decay channel K*(0) -> K +/-pi -/+. Measurements of transverse-momentum integrated yield, mean transverse--momentum, nuclear modification factor of K*(0),and yield ratios of resonance to stable hadron (K*(0)/K) are compared across different collision systems (pp, p-Pb, Xe-Xe, and Pb-Pb) at similar collision energies to investigate how the production of K*(0) resonances depends on the size of the system formed in these collisions. The hadronic rescattering effect is found to be independent of the size of colliding systems and mainly driven by the produced charged-particle multiplicity, which is a proxy of the volume of produced matter at the chemical freeze-out. In addition, the production yields of K*(0) in Xe-Xe collisions are utilized to constrain the dependence of the kinetic freeze-out temperature on the system size using the hadron resonance gas-partial chemical equilibrium model.

PHYSICAL REVIEW C 109[1], 014911, 2024. DOI: 10.1103/PhysRevC.109.014911

[P053-2024] "The absorption spectrum of the H24O radioactive isotopologue of water vapour"

Voronin, B. A.*; Tennyson, J.; Chesnokova, T. Y.; Chentsov, A. V.; Bykov, A. D.

The predicted rotation-vibration absorption spectrum of the radioactive isotopically substituted water molecule, (H2O)-O-14, is presented. Variational nuclear-motion calculations are performed using the DVR3D software package based on the use of a high-precision potential energy function and an accurate dipole moment surface. Line centres, intensity and Einstein coefficients are calculated, and air pressure broadening coefficients are estimated. The calculation was carried out over a wide wavenumber range from 0 to 25000 cm-1-1 and total angular momentum up to J = 20. Isotopologue extrapolation rules based on experimentaldata on the energy levels of the stable isotopologues (H2O)-O-16, H162216O (H2O)-O-17 and (H2O)-O-18 were also used to improve the predicted line positions. Spectral ranges best suited to the detection of (H2O)-O-14 are identified.

MOLECULAR PHYSICS, 2024. DOI: 10.1080/00268976.2024.2333474 **Early Access:** MAR 2024

[P054-2024] "The functional generalization of the Boltzmann-Vlasov equation and its gauge-like symmetry"

Torrieri, G.*

We argue that one can model deviations from the ensemble average in non-equilibrium statistical mechanics by promoting the Boltzmann equation to an equation in terms of functionals , representing possible candidates for phase space distributions inferred from a finite observed number of degrees of freedom. We find that, provided the collision term and the Vlasov drift term are both included, a gauge-like redundancy arises which does not go away even if the functional is narrow. We argue that this effect is linked to the gauge-like symmetry found in relativistic hydrodynamics [1] and that it could be part of the explanation for the apparent fluid-like behavior in small systems in hadronic collisions and other strongly-coupled small systems [2]. When causality and Lorentz invariance are omitted this problem can be look at via random matrix theory show, and we show that in such a case thermalization happens much more quickly than the Boltzmann equation would infer. We also sketch an algorithm to study this problem numerically.

SCIPOST PHYSICS 16[3], 070, 2024. DOI: 10.21468/SciPostPhys.16.3.070

[P055-2024] "Vector-like singlet quarks: A roadmap"

Alves, J. M.; Branco, G. C.; **Cherchiglia, A. L.***; Nishi, C. C.; Penedo, J. T.; Pereira, P. M. F.; Rebelo, M. N.; Silva-Marcos, J. I.

We review the theory and phenomenology of isosinglet vector--like quarks (VLQs). In recent years, interest in VLQs has been increasing, due to their contributions to new physics effects that can be tested in experiments at LHC and High-Luminosity LHC. The similarities of models with isosinglet VLQs and the seesaw framework in the leptonic sector are pointed out. The existence of VLQs leads to flavour-changing neutral currents at tree level and deviations from unitarity of the CKM matrix, introducing rich phenomenological implications. These new effects are naturally suppressed by the masses of the new quarks, that are constrained to be above the electroweak scale. In addition, striking new effects can be achieved with the inclusion of an extra complex scalar singlet. Such a minimal extension of the SM can give rise to new sources of CP violation with profound theoretical implications, allowing for a solution to the strong CP problem and a possible explanation for the baryon asymmetry of the Universe. We list and explain strong motivations to consider this class of models. We also briefly review how models with VLQs can be matched to the SM effective field theory (SMEFT). A detailed analysis of flavour observables that can be affected by the presence of VLQs is presented. Current bounds from collider searches of VLQs are summarized. We point out that the discovery of VLQs can be within the reach of present or future colliders being planned.

PHYSICS REPORTS-REVIEW SECTION OF PHYSICS LETTERS 1057, 1-69, 2024. DOI: 10.1016/j.physrep.2023.12.004

[P056-2024] "ZnO/CeO2/carbon xerogel composites with direct Z-scheme heterojunctions: Enhancing photocatalytic remediation of 4-chlorophenol under visible light"

Moraes, N. P. de; Sanmartin, M. B. de C.; Rocha, R. da S.; **Siervo, A. de***; Lanza, M. R. de V.; Reddy, D. A.; Yu, L. Q.; Rodrigues, L. A.

This paper aims to create visible light driven ternary photocatalysts using zinc oxide (ZnO), cerium (IV) oxide (CeO2), and carbon xerogel (CX) as constituent materials. The use of CeO2 is based on the creation of direct -Z -scheme heterojunctions with the ZnO and the consequent diminishing of charge recombination, whereas the carbon xerogel inclusion is predicted to minimize bandgap energy, decrease electron -hole recombination, and boost specific surface area. Furthermore, the choice of the black -wattle tannin as a carbonaceous precursor was targeted at the development of an environmentally friendly and affordable composite. The existence of the hexagonal phase of zinc oxide and cubic structure of the cerium (IV) oxide in the ternary material was confirmed by X-ray diffractometry and X-ray photoelectron spectroscopy, with the latter also suggesting chemical bonding between the ZnO and the CX due to the creation of zinc oxycarbide complexes. The inclusion of the carbon xerogel provokes a significant modification in the morphology of the ternary material, resulting in an increased surface area and smaller particle aggregates. The CX/ZnO-CeO2 ternary composite obtains the highest photocatalytic efficiency among all the materials studied, degrading 100% of 4-chlorophenol under simulated sunlight and 68% under visible radiation, after 5 h. The increased photocatalytic activity can be attributed to the formation of direct Z -scheme heterojunctions between the semiconductors, higher visible light response, and higher specific surface area, as evidenced by the results obtained by active radical scavenging, chronoamperometry, diffuse reflectance spectroscopy, and N2 adsorption -desorption isotherms. 0 2022 Chinese Society of Rare Earths.

JOURNAL OF RARE EARTHS 42[2], 314-322, 2024. DOI: 10.1016/j.jre.2022.11.001

***Autores da comunidade IFGW**
Fonte: Web of Science on-line (WOS)

Defesas de Dissertações do IFGW

[D007-2024] "Métodos analíticos para a formulação da oscilação de neutrinos"
Aluno: Carlos Javier Gomez Fuentes
Orientador: Prof. Dr. Orlando Luís Goulart Peres
Data: 23/04/2024

[D008-2024] "Identificação de Inomogeneidades Morfológicas e Espectrais em Perovskitas de Haleto de Metal"
Aluno: Charles Alves Nogueira de Almeida
Orientador: Prof. Dr. Luiz Fernando Zagonel
Data: 29/04/2024

[D009-2024] "Separação de chuveiros eletromagnéticos em LArTPCs: estudo do método calorimétrico no LArIAT"
Aluno: Maria Gabriela Manuel Alves
Orientador: Prof. Dr. Ernesto Kemp
Data: 02/05/2024

[D010-2024] "Otimização Online da Abertura Dinâmica do SIRIUS"
Aluno: Matheus Melo Santos Velloso
Orientador: Prof. Dra. Liu Lin
Data: 03/05/2024

Defesas de Teses do IFGW

[T004-2024] "Otimização de cristais optomecânicos híbridos e efeitos termo-optomecânicos"
Aluno: Cauê Moreno Kersul de Castro Carvalho
Orientador: Prof. Dr. Thiago Pedro Mayer Alegre
Data: 22/03/2024

[T005-2024] "Materiais quânticos complexos na estrutura cristalina dos 112"
Aluno: Gabriel Silva Freitas
Orientador: Prof. Dr. Pascoal José Giglio Pagliuso
Data: 19/04/2024

[T006-2024] "Modelagem teórica de monocamadas anfifílicas: gás de rede de Doniach em redes tripartidas na aproximação de pares"
Aluno: Carolina Paz Barateiro Vignoto
Orientador: Prof. Dr. Mario Noboru Tamashiro
Data: 22/04/2024

Fonte: Portal IFGW/Eventos
Disponível em: https://portal.ifi.unicamp.br/a-instituicao/eventos/month.calendar/2023/12/14/-

Defesas de Dissertações e Teses do PECIM

[P002-2024] "Percepções de alguns formadores sobre ações entre 2012 a 2021: o olhar dos formadores sobre os processos formativos da Diretoria de Ensino Campinas Oeste"
Aluno: Paulo Rogério da Silva
Orientador: Prof. Dr. Gildo Girotto Júnior
Banca: Prof Dr Mauricio Compiani - IG/Unicamp (Presidente), Profa Dra Ivana Elena Camejo Aviles - IB/Unicamp, Prof Dr **Guilherme Stecca Marcom - IFGW/Unicamp,** Profa Dra Ana de Medeiros Arnt - IB/Unicamp (Suplente), Profa Dra Dora Maria Grassi Kassisse - IB/Unicamp (Suplente)
Data: 05/04/2024
Exame de Defesa: Doutorado

Fonte: Página do PECIM
Disponível em: https://www.pecim.unicamp.br/bancas

Abstracta

Instituto de Física
Diretor: Profa. Dra. Mônica Alonso Cotta
Diretora Associada: Prof. Dr. Marcos Cesar de Oliveira
Universidade Estadual de Campinas - UNICAMP
Cidade Universitária Zeferino Vaz
13083-859 - Campinas - SP - Brasil
e-mail: secdir@ifi.unicamp.br
Fone: +55 19 3521-5300

Publicação

Biblioteca do Instituto de Física Gleb Wataghin
http://portal.ifi.unicamp.br/biblioteca
Instagram: @bif.unicamp

Diretora Técnica: Sandra Maria Carlos Cartaxo
Coordenadora da Comissão de Biblioteca: Profa. Dra. Arlene Cristina Aguilar

Elaboração e editoração:
Maria Graciele Trevisan (Bibliotecária)
Artes gráficas: Júlia da Silva Oliveira (Estagiária)
Contato: infobif@ifi.unicamp.br